Talanta xxx (xxxx) xxxx

Contents lists available at ScienceDirect

Talanta

journal homepage: www.elsevier.com/locate/talanta

Combination of area controllable sensing surface and bipolar electrode-electrochemiluminescence approach for the detection of tetracycline

Longsheng Jin, Jingtang Qiao, Jinghan Chen, Ning Xu, Meisheng Wu*

Department of Chemistry, College of Sciences, Nanjing Agricultural University, 1 Weigang, Nanjing, 210095, PR China

ARTICLE INFO

Keywords:
Closed bipolar electrode
Electrochemiluminescence (ECL)
Area-controllable sensing interface
Biosensor

ABSTRACT

A novel area controllable biosensing interface is designed on glassy carbon bead (GCB) and used for measurement of tetracycline (TET) in closed bipolar electrode-electrochemiluminescence (ECL) device. One face of GCB is modified with Au particles and the covered area is varied from 0 to 45.3% by tuning the external voltage during bipolar electrodeposition process in a home-made open bipolar electrochemical cell. It enables the conjugation of various amounts of biomolecules on Au/GCB. Then DNA walker and methylene blue (MB) labeled DNA (MB-DNA) are conjugated on Au surface for the following combination of aptamer. In the presence of target, aptamer partially hybridized with DNA walker will be released from Au surface, leading to the formation of dsDNA between DNA walker and MB-DNA. As a result, MB-DNA with recognition site for nicking endonuclease (Nb.*Bbv*CI) in dsDNA is cleft into two segments by Nb.*Bbv*CI. Meanwhile, the liberated DNA walker is triggered to continue the degradation of many MB-DNA. Due to the excellent electrochemical performance of MB, it is reduced at the cathode of BPE to amplify the ECL signal at the anode of BPE in a closed BPE-ECL platform. When the covered area of GCB by Au particles is enlarged from 10.1 to 45.3%, the change of ECL intensity could be increased 2.7-fold. The linear range for the detection of tetracycline is from 1×10^{-12} to 1×10^{-5} M with the detection limit of 6.0×10^{-13} M. Hence, controllable sensing area on a single glassy carbon bead, the amplification effect of DNA walker and MB make this approach possess many advantages over traditional biosensor.

1. Introduction

Bipolar electrochemistry, as a powerful technique, has attracted more and more attention in recent years due to its unique properties [1–19]. Electrochemical reactions are taken place at the anodic pole and cathodic pole of bipolar electrode (BPE) at the same rate to maintain the charge neutrality of it if a sufficient high voltage is applied in the solution [20–27]. Therefore, the oxidation reactions occurred at the anode can be used to report the reduction reactions at the cathode. The current flowing through BPE can be reported by electrochemiluminescent (ECL) [4–6], colorimetric approach [28], and fluorescent [10,29]. In order to perform diverse tasks, versatile BPE platforms have been designed, such as light-emitting electrochemical cells [2], paperfluidic devices [3], ITO glass substrate [4], and cloth-based devices [6]. Xu's group has developed a novel BPE device on a single electrode based on resistance induced potential difference [30]. Importantly, the anode and cathode can be composed of two distinct electrode materials in a closed BPE device which enables the specific fabrication of functional interface at these two electrodes and avoids the chemical interface in electrochemical cells. Since ECL involves electrochemical reactions and the following luminescence process, it has been emerged as an attractive strategy to report the electrochemical reactions occurred at BPE. The combination of closed BPE-ECL has been utilized in designing versatile biosensors [6,31–35], screening of catalysts [36], and multiplexed sensing on the basis of BPE array [31,37,38]. For example, Xu's group has developed a novel visual ECL ratiometry biochip for biomarker measurement [4]. The excellent quenching effect of Au nanorods on the ECL of CdTe quantum dots (QDs) at the cathode of BPE led to the decreased current across BPE and the reduced ECL signal emitted from luminol at the anode of BPE. The concentration of target can be easily analyzed by the ratio of green-colored ECL of CdTe (QDs) and blue-colored ECL of luminol.

Taking advantage of BPE, versatile effective strategies have been developed to broaden the applications of electrochemistry and realize sensitive detection. The integration of catalysts at the cathode of BPE can amplify the reduction current by improving its conductivity and surface area, for instance, multi-walled carbon nanotubes/graphene quantum dots-gold nanoparticles [6] and Au nanoparticles (NPs)

* Corresponding author.
E-mail address: wumeisheng@njau.edu.cn (M. Wu).

https://doi.org/10.1016/j.talanta.2019.120404
Received 10 June 2019; Received in revised form 24 September 2019; Accepted 27 September 2019
0039-9140/ © 2019 Elsevier B.V. All rights reserved.

labeled DNA [39]. Besides, study has also revealed that the electrochemical signal is closely related with the electrode size [37]. As the increasing of cathode size, the current flowing through BPE is enhanced, leading to an improved ECL signal at the anode of BPE [37]. Xu has revealed that the ECL intensity emitted at the anode of BPE is increased when the width of BPE is increased from 2 mm to 4 mm and then decreased promptly with the further increasing of BPE width [40]. Furthermore, bringing electroactive species into close proximity with cathode surface through specific recognition reactions allows the generation of an improved reduction current, leading to an enhanced signal at BPE [41]. Therefore, if the reduction of electroactive species are impeded, the ECL signal will be inhibited accordingly [42].

Inspired by the influence of electrode size on ECL signal in BPE device, we design a novel platform based on the combination of controllable sensing interface on a single glassy carbon bead (GCB) and DNA walker-assisted amplification effect. A size controllable sensing interface prepared by bipolar electrochemical technique is employed to load large number of biomolecules which eliminates the fabrication of BPE with various sizes. The sensing coverage area is designed to vary from 0 to 45.3% through bipolar plating of Au particles on one face of GCB array in a home-made open bipolar electrochemical cell according to our previous work [43]. As a result, the modification amount of biomolecules is improved remarkably compared to traditional strategies. In this work, tetracycline (TET), one of the important broad-spectrum antibiotics [44,45], is utilized as an example to evaluate the performance of the developed biosensor. Methylene blue labeled DNA (MB-DNA) and DNA walker which is partially complementary with aptamer are functionalized on Au surface. Upon the introduction of target (TET), aptamer is released from Au surface, leading to the hybridization of DNA walker with MB-DNA. As a result, MB-DNA with recognition site for nicking endonuclease (Nb.*Bbv*CI) in dsDNA is cleft into two segments, causing the separation of MB from GCB surface. Meanwhile, the liberated DNA walker is triggered to continue the degradation of residual MB-DNA. Due to the excellent reduction performance of MB, the above solution is then exposed to the cathode of closed BPE-ECL setup to trigger the oxidation of ECL reagents at the anode of BPE. Results have indicated that the ECL signal can be detected by using a single GCB and the intensity is closely related to the coverage area of Au. So it is believed that the proposed strategy shows great potential in sensitive and convenient detection by pre-modifying biomolecules on GCB.

2. Experimental section

2.1. Materials and reagents

$HAuCl_4$ was from Sinopharm chemical reagent company (Shanghai, China). $Ru(bpy)_3^{2+}$, 6-mercapto-1-hexanol (MCH), tris(2-carboxyethyl) phosphine hydrochloride (TCEP) were obtained from sigma-Aldrich. Tetracycline (TET) was purchased from Aladdin Chemical Shanghai Co., Ltd. Glassy carbon spherical powder (GCB, type 2, diameter of 630–1000 μm) was from Alfa Aesar. All the other chemicals were of analytical grade. DNA oligonucleotides were provided by Sangon Biotech Co. Ltd. (Shanghai, China) and the sequences were displayed as follows.

TET aptamer: 5′-TGAGGCGTACGGAATTCGCTAGCCCCCCGGCAGGCCACGGCTTGGGTTGGTCCCACTGCGCGTGGATCCGAGCTCCACGTG-3'.

TET walker: 5′–SH–$(CH_2)_6$-T-46-GGGGGGCTAGCGAATTCCGTACGCCTCAGC-3'.

MB-DNA: 5′–SH–$(CH_2)_6$-T-6-T***GC*TGAGG***-methylene blue-3'.

MB-DNA-4: 5′–SH–$(CH_2)_6$-T-6-T***GC*TGAGG***TT-methylene blue -3'.

MB-DNA-8: 5′–SH–$(CH_2)_6$-T-6-T***GC*TGAGG***TTGGTTGG-methylene blue -3'.

Bold region represented the nicking recognized sequence. * was the cutting site of Nb.*Bbv*CI [46]. Underline represented the complementary region of DNA.

Indium tin oxide (ITO)-coated (thickness, ~100 nm; resistance, ~10 Ω/square) aluminosilicate glass slides were purchased from CSG (Shenzhen, China). Sylgard 184 (including polydimethylsiloxane (PDMS) monomer and curing agent) was obtained from Dow Corning (Midland, MI, USA).

2.2. Instruments

ECL signals were recorded with MPI-E multifunctional electrochemical and chemiluminescent analytical system (Xi'an Remax Electronic Science &Technology Co. Ltd., Xi'an, China). Two Pt wires were placed at the two reservoirs and connected with the above instrument to supply voltage for driving the electrochemical reactions occurred at ITO BPE. A DC power supply (eTM-300W, Etommens Electronic Technology Co. Ltd., Dongguan, China) was connected with two Pt plate electrodes (1.5 cm × 2.0 cm) to achieve bipolar deposition of Au particles at one face of GCB array. The morphologies of Au particles modified GCBs were characterized by scanning electron microscopy (S-3400N II). UV–vis absorption spectra were obtained on NanoDrop (ND-ONEC-W, Thermo Fisher Scientific) spectrophotometer.

2.3. Bipolar deposition of Au on GCBs array in open bipolar electrochemical cell

The deposition of Au particles with controllable surface coverage on one face of GCBs has been reported in our previous work [43]. The setup was depicted in Scheme 1A. In open bipolar electrochemical cell, although the voltage applied at the two ends of BPE is smaller than that in closed BPE cell, the whole BPE is immersed into solution which enables the simultaneous detection and modification of nanoparticles on one face of BPE array at the same time. In order to decrease the deposition voltage for Au and enlarge its surface area, big and uniform size of GCB with diameter of 750 μm was selected and washed with acetone and water, followed by drying under 100 °C for 1.5 h.

A 4 × 14 GCB array was fabricated on glass substrate and then placed in a home-made electrochemical cell (2.5 cm of length, 1.5 cm of width, and 1.5 cm of height). 2 mL of 10 mM $HAuCl_4$ was added into the electrochemical cell and an external voltage ranged from 12 to 32 V was applied on two Pt plate electrodes with a distance of 1.5 cm to drive the bipolar deposition of variable area of Au on GCB. After that, these Au/GCBs were rinsed with water for three times and dried at room temperature for future use.

2.4. Fabrication of closed bipolar electrochemical cell

ITO glasses (30 mm × 30 mm) were sequentially sonicated in 10 g/L alconox aqueous solution for 15 min, propan-2-ol for 15 min, and twice in water for 15 min. Then they were dried at 60 °C. After these cleansing procedures, a negatively charged ITO electrode was obtained [47].

The closed BPE device for the detection of DNA was fabricated according to the following procedures. It consisted of two layers of PDMS slices and the as-prepared ITO electrode. Two reservoirs with a diameter of 3 mm were punched on each PDMS slice. The centre-to-centre distance of reservoirs at the bottom and top layer of PDMS slice were 7 and 9 mm, respectively. Pt wires were placed in the two reservoirs of top PDMS slice and connected to MPI-E multifunctional electrochemical and chemiluminescent analytical system. ITO electrodes in the two holes of bottom PMDS slice were acted as the cathodic and anodic pole of BPE.

2.5. Fabricating biosensing interface on Au/GCB surface and ECL detection

50 μL of 1 μM MB-DNA was mixed with the same volume of 1 μM TET walker and 1.5 μL of 50 μM tris- (2-carboxyethyl) phosphine hydrochloride (TCEP) at 37 °C for 2 h to cleave the disulfide bonds. Then 90 μL of the above solution was incubated with Au/GCB at 37 °C for 4 h.

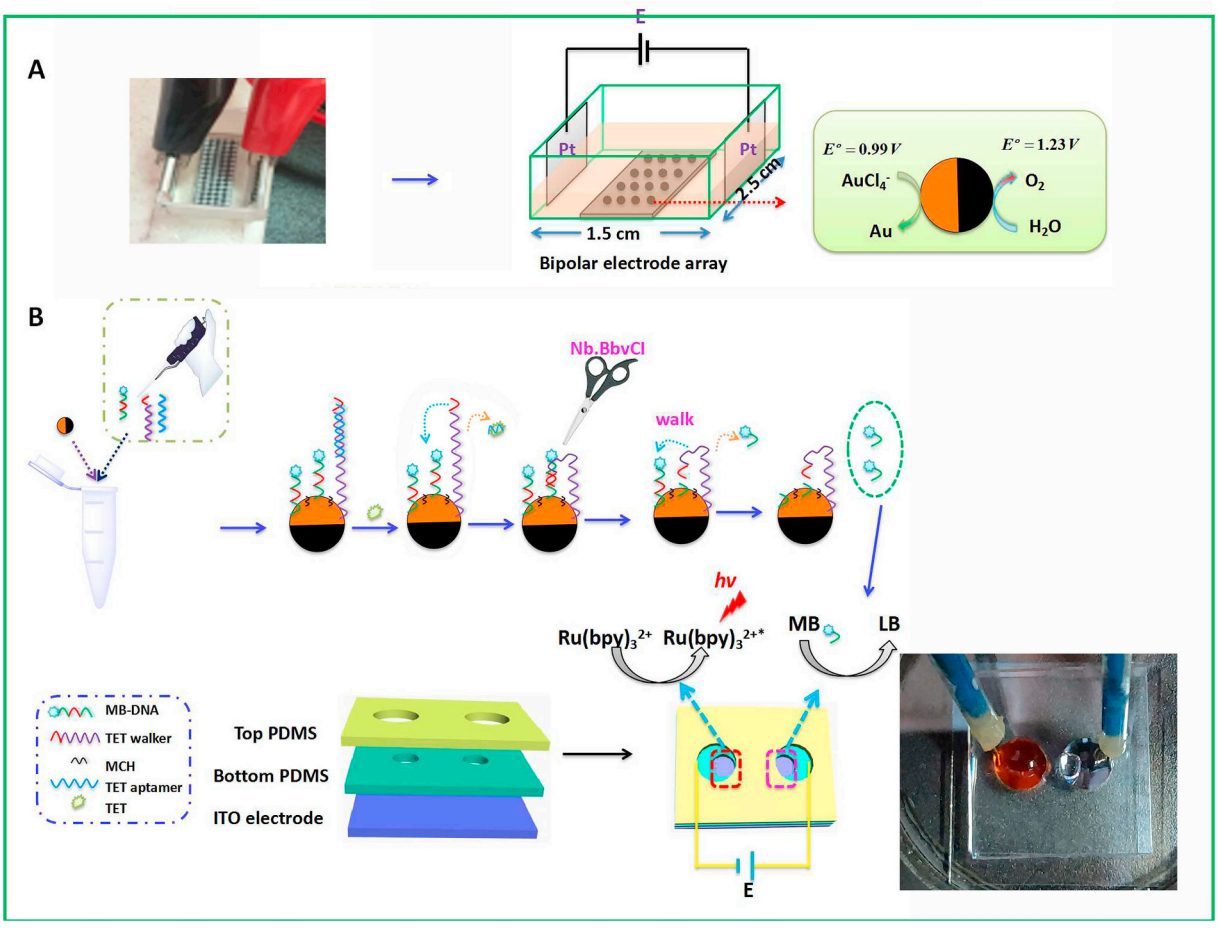

Scheme 1. (A) Open bipolar electrochemical cell for the deposition of Au particles on one face of GCB array. (B) Scheme diagram of sensing principle with Au/GCB biosensor and detecting mechanism in a closed BPE-ECL device.

After rinsing with PBS, the active sites on Au/GCB were blocked by immersing it in 90 µL of 1.0 µM mercaptohexanol (MCH) at 37 °C for 30 min. The prepared MCH/MB-DNA- TET walker/Au/ITO was then washed with PBS and incubated with 100 µL of 1 µM TET aptamer at 37 °C for 1 h. Finally, it was carefully washed with PBS and immersed into 100 µL of mixture solution of 0.5 µM TET and Nb.*Bbv*CI (5 U/50 µL, NE Buffer (1 ×)) at 37 °C for 2 h.

The above solution was then transferred to the right reservoir of closed BPE platform. The left reservoir was filled with 100 µL PBS solution containing 2 mM $Ru(bpy)_3^{2+}$ and 20 mM DBAE. A cyclic voltage from 0 to 3.3 V was applied at the two Pt wires to trigger the redox reactions at ITO electrodes in these two reservoirs.

2.6. UV characterization

In order to improve the UV–vis absorbance, the concentration of each solution was increased to 5 times and 5 Au/GCBs (prepared under the deposition voltage of 32 V) was immersed into DNA solution. UV–vis spectra of solution were evaluated by NanoDrop spectrophotometer.

2.7. Analysis TET concentration in real sample

50 µL of milk samples were diluted with 9.95 mL of PBS. Then various concentration of TET standard solution was spiked into 25 µL of the diluted milk solutions, respectively. The concentration of TET was measured with the designed biosensor.

3. Results and discussion

3.1. Principle of the biosensor

The deposition of Au nanoparticles at one face of GCB was similar to our previous study [43] (Scheme 1A). It was a typical open bipolar electrochemical cell in which the whole GCBs are placed into solution and an external voltage was applied on two Pt plate electrodes (driving electrodes) to trigger the reduction of $AuCl_4^-$ on the cathode of GCB BPE and the oxidation of H_2O on the opposite side of GCB BPE. Due to the unique advantages of open bipolar electrochemistry, large number of Au/GCBs could be prepared simultaneously by fabricating GCB array. Since no electric connection between BPE and the power source, the potential difference obtained at the two ends of BPE was controlled by the magnitude of electric field in the solution and the size of GCB (BPE). Therefore, the deposition area of Au on GCB could be easily tailored by the voltage, resulting in a tunable area for the conjugation of biomolecules. So each Au/GCB could be acted as an independent biosensor (Scheme 1B). Au/GCB was then immersed into a mixture solution of TET walker and MB labeled DNA (MB-DNA). MB-DNA was designed to contain the sequence of 5' -GCTGAGG-3' which can be recognized and cleft by Nb.*Bbv*CI nicking enzyme.TET walker was then hybridized with aptamer to form duplex DNA in order to avoid the non-specific hydrolysis of MB-DNA by Nb.*Bbv*CI. When TET was introduced into the solution, TET aptamer was released from Au/GCB surface due to the high affinity between them. Then TET walker was triggered to hybrid with MB-DNA. The duplex DNA was recognized by Nb.*Bbv*CI and MB-DNA was separated into two segments. As a result, MB labeled fragment was released from Au/GCB surface and TET walker entered

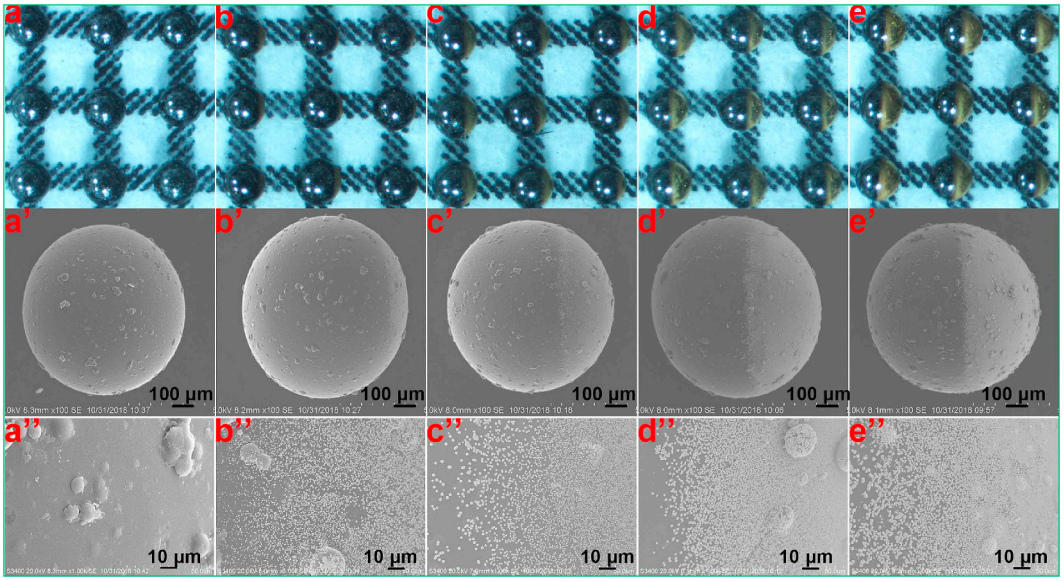

Fig. 1. (a to e) Optical images of GCB array under various deposition voltages of Au. (a' to e' and a'' to e''). The corresponding SEM images of Au/GCB. The deposition voltages from a to e were 12, 17, 22, 27, and 32 V, respectively. The concentration of $HAuCl_4$ was 10 mM.

the next cycle of walking. The reaction solution was added to the right reservoir of closed BPE device and ECL solution was added into the left reservoir. In this device, the chemical interface between the reaction solution and ECL reagent could be avoided. Additionally, previous studies have revealed that the potential difference obtained on the two ends of BPE in closed BPE cell is larger than that in open BPE cell [31]. Thus, this device was chosen as a good choice for the ECL detection. Then a voltage was applied between these two reservoirs to trigger the oxidation of $Ru(bpy)_3^{2+}$/DBAE at the part of ITO in the left reservoir and the reduction of MB at the other part of ITO.

3.2. Characterization of Au/GCB

Fig. 1 displayed the optical images (a to e) and SEM images (a' to e' and a'' to e'') of Au/GCB prepared through bipolar electrodeposition technique. The diameter of GCB used in this work was about 750 μm. Therefore, the minimum voltage for the reduction of $AuCl_4^-$ at the terminal of GCB was 4.8 V according to the following equation [20].

$$\Delta E_{elec} = \frac{l_{BPE}}{l_{channel}} \Delta E_{tot}$$

Here, ΔE_{elec} is the potential difference obtained at the two poles of BPE. ΔE_{tot} refers to the external voltage applied at the driving electrodes. l_{BPE} denotes the length of BPE (diameter of GCB). $l_{channel}$ is the distance between driving electrodes.

However, ΔE_{elec} is also affected the conductivity of the solution [48], the resistance of bipolar electrode [49], and the charge transfer resistance at driving electrode/solution interface [31]. As can be seen from Fig. 1 (a, a' and a'') that no obvious particles could be observed at GCB when the deposition voltage was 12 V. With the increase of external voltage (from b to e), plenty of Au particles could be seen at one side of GCB and the coverage area of it was extended gradually from the end to the centre of GCB. About 45.3% of GCB was covered by Au particles when the deposition voltage reached 32 V. The area of Au cap on GCB can be calculated according to the following equation.

$$S_{cap} = 2\pi Rh$$

R represented the radius of GCB which was approximately 375 μm h denoted the height of Au cap.

Therefore, the area of Au cap was increased from 0.117 to 0.400 mm^2 when the deposition voltage of Au was increased from 17 V to 32 V.

Besides, the diameter of Au particle was also increased as the increase of deposition voltage (b'' to e''). It was increased from 0.65 to 1.45 μm when the deposition voltage increased from 17 to 32 V due to the accelerated deposition rate of Au under high voltage.

3.3. MB modulated ECL signal in BPE system

Previous studies have indicated that the reduction of electroactive species can improve the number of electron flowing through BPE and enhancing the ECL signal at the opposite pole of BPE [20]. Additionally, the voltage applied at the two ends of BPE in open BPE cell is lower than that in closed BPE cells [31]. Therefore, in order to achieve sensitive detection, we studied the performance of MB modulated ECL signal in closed BPE platform. Fig. 2A was the cyclic voltammogrames performed with a 3-electrode setup when the working electrode (bare ITO electrode) was immersed into PBS and MB solution, respectively. MB displayed a pair of reduction and oxidation peaks at *ca.* −0.24 and −0.20 V. It suggested that the reduction of MB at the cathode of ITO BPE could improve the number of electron flowed through BPE, leading to an amplified ECL signal at the anode of BPE.

Fig. 2B was the corresponding ECL-voltage curves obtained in closed BPE-ECL device. The ECL intensity was increased promptly when the voltage was higher than 2.5 V (curve a) due to the reduction of oxygen at the cathode of BPE and the oxidation of $Ru(bpy)_3^{2+}$/DBAE at the anode of BPE. As expected, an enhanced ECL intensity was obtained after the introducing of MB at the cathode of BPE (curve d), ascribing to the reduction of MB instead of oxygen which decreased the onset voltage and amplified the oxidation reaction at the anode. In order to confirm that the reduction of MB can be used in bioanalysis, the cathode of BPE was exposed into MB-DNA solution. As expected, the ECL intensities obtained in the presence of 1 nM (b) and 1 μM (c) MB-DNA were higher than that in PBS (a) and the intensity was increased as the concentration of MB-DNA, confirming that MB labeled at the terminal of DNA could be employed for the designation of biosensor. Meanwhile, the ECL intensity in the presence of 1 μM MB was higher than that in the solution of MB-DNA, attributing to the electrostatic repulsion between DNA backbone and the negatively charged ITO electrode.

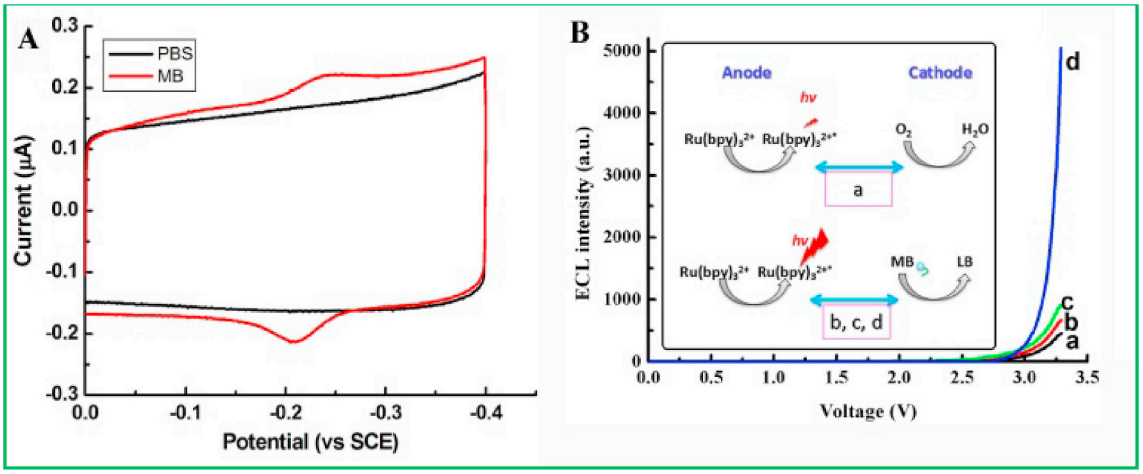

Fig. 2. (A) Cyclic voltammogrames of bare ITO electrode in PBS and 1 μM MB. The working area of ITO electrode was 0.24 cm^2. The scan rate was 0.05 V/s. (B) ECL-voltage curves obtained in closed-BPE device. The anode of ITO BPE was immersed into $Ru(bpy)_3^{2+}$/DBAE solution and the cathode of it was exposed to PBS (a), 1 nM MB-DNA(b), 1 μM MB-DNA(c), and 1 μM MB (d), respectively.

3.4. Characterization of the biosensor

The hybridization process and the cleavage of MB-DNA on Au-GCB were characterized by UV–vis absorption spectroscopy. For comparison, naked GCBs were treated with the same solutions. Fig. 3A was the UV–vis spectra of mixture solution of MB-DNA and TET walker after incubating with GCB (a) and Au/GCB (b). Two distinct absorption bands located at ca. 263 and 664 nm could be observed in these two solutions. The first peak was attributed to the absorption of DNA and the second one was caused by MB which could be confirmed by the spectrum of MB-DNA(c) and DNA walker (d). These two peaks in solution containing Au/GCB were lower than that in naked GCB, confirming that MB-DNA was successfully conjugated on Au surface of GCB.

The above two types of GCBs were washed with PBS and then immersed into TET aptamer, the absorption spectra were displayed in Fig. 3B. Only an absorption peak located at 260 nm can be seen in both Au/GCB (curve a) and GCB (curve b). Additionally, the absorbance of solution containing Au/GCB was dropped remarkably compared to that in GCB, indicating that aptamer was specifically captured on Au/GCB surface through the formation of duplex with TET walker because the active sites on Au was blocked by MCH prior to the incubation of aptamer. Followed by rinsing with PBS, the above Au/GCB and GCB were immersed into the mixture solution of TET and Nb.*Bbv*CI to trigger the walking of TET walker and the detection of TET. Results were presented in curve c (Au/GCB) and curve d (GCB) in Fig. 3B. Unfortunately, no obvious absorption peak ascribing to MB can be seen in Au/GCB (curve c) which might cause by the low concentration of MB functionalized on Au surface (see from Fig. 3A). However, the absorbance at 260 nm in the solution containing GCBs was higher than that of Au/GCBs, confirming that MB-DNA was cleft and released from Au/GCB surface in the presence of TET and Nb.*Bbv*CI.

3.5. Optimization of the experimental conditions

The ratio between TET walker and MB-DNA was one of the important factors that influenced the hybridization and cleavage efficiency. Therefore, equivalent volume of various concentration of TET walker was mixed with 1.0 μM MB-DNA to investigate the effect of ratio on the ECL intensity. As can be seen from Fig. 4A, the ECL intensity increased with the increasing ratio of TET walker and MB-DNA and then reached highest value when the ratio was 1/15. After that, the ECL intensity was dropped apparently. Thus, in order to improve the sensitivity of the designed biosensor, a ratio of 1/15 was selected for DNA walking and DNA measurement.

Fig. 4B was the ECL response on the concentration of MB-DNA. With the increase of its concentration, ECL intensity increased dramatically due to the increased amount of MB liberated from Au/GCB surface after

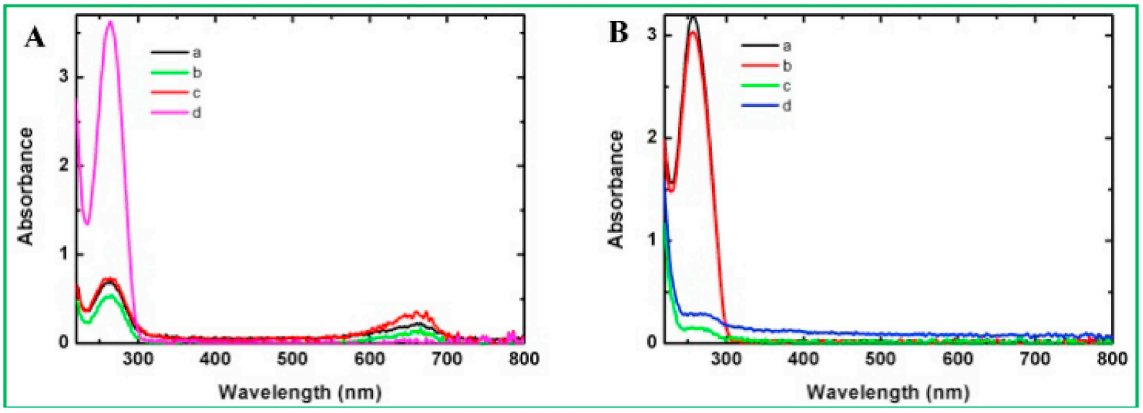

Fig. 3. (A) UV–vis absorption spectra of mixture solution of MB-DNA (2.5 μM) and TET walker (2.5 μM) incubated with GCB (a) and Au/GCB (b) for 4 h. UV–vis absorption spectra of MB-DNA (c) and TET walker (d). (B) UV–vis absorption spectra of aptamer (5 μM) incubated with TET walker/MB-DNA/Au/GCB (a) and GCB (b) for 1 h. Subsequently, mixture solution of TET (2.5 μM) and Nb.*Bbv*CI (12.5 U/μL, NE Buffer (1 ×)) were incubated with aptamer/TET walker/MB-DNA/Au/GCB (c) and GCB (d).

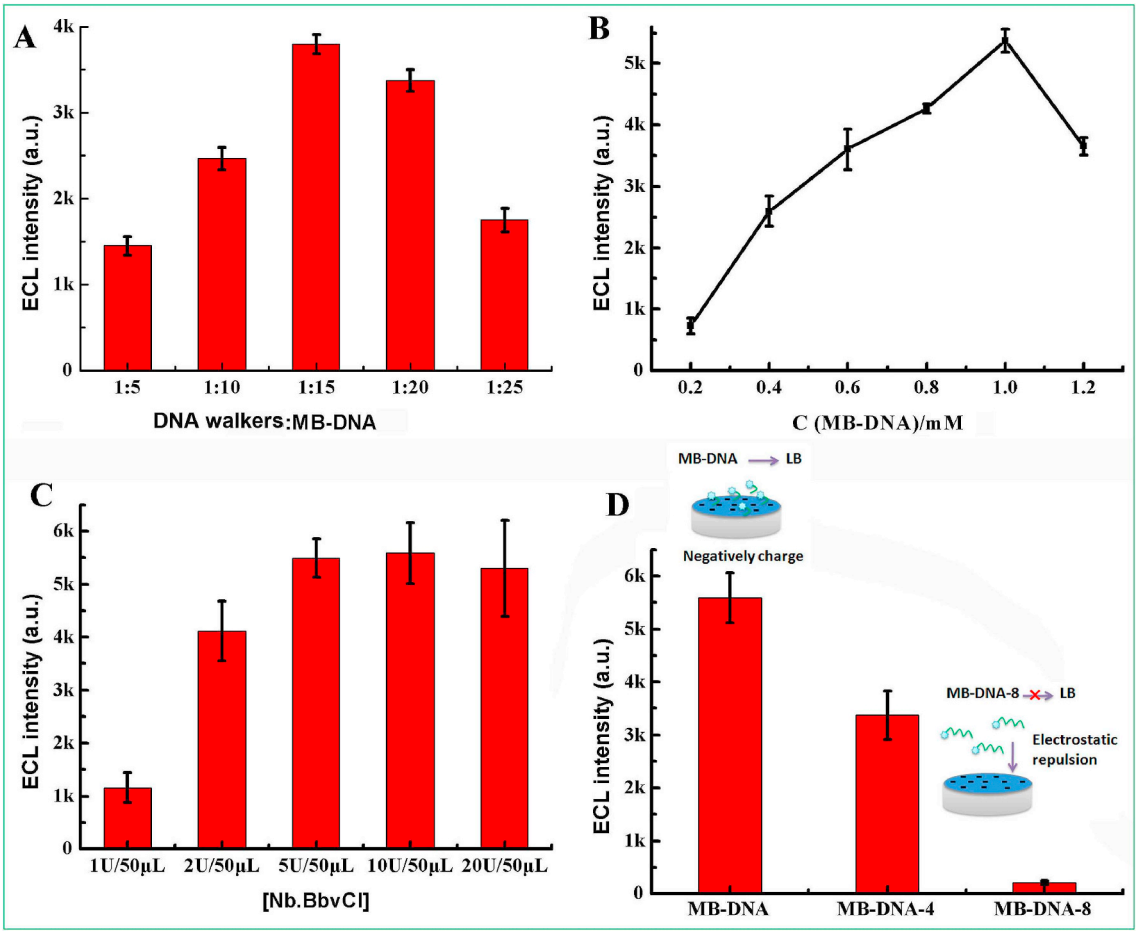

Fig. 4. The effect of the ratio of DNA walkers and MB-DNA(A), MB-DNA concentration (B), Nb.*Bbv*CI concentration (C) on the ECL intensity. (D) The influence of the number of bases between MB and the cleavage site on the ECL intensity. Error bars represented the standard deviation of three measurements.

the splitting of MB-DNA. Then the intensity was decreased when it was higher than 1.0 μM because the enhanced density of MB-DNA on Au/GCB surface might impede the following hybridization and cleavage efficiency. Therefore, 1.0 μM was chosen as the optimal concentration.

Nb.*Bbv*CI was employed to cut all hybridized MB-DNA and release MB into solution for the following ECL measurement. The effect of Nb.*Bbv*CI concentration on the ECL signal was demonstrated in Fig. 4C. It displayed that the ECL intensity was increased obviously and then level off when the concentration of Nb.*Bbv*CI reached 5 U/50 μL. Hence, it was selected as the optimal concentration for the degradation of MB-DNA.

We also investigated the number of bases between MB and the cleavage site of Nb.*Bbv*CI in MB-DNA on the ECL intensity. As presented in Fig. 4D, the ECL intensity dropped promptly to 3.65% when the number of based was increased from 0 to 8, attributing to the improved electrostatic repulsion between the negatively charged backbone in MB-DNA fragment and the same charge ITO electrode which impeded the contact of MB-DNA fragment with ITO electrode. Therefore, the ECL intensity was very sensitive to the number of bases in the fragment of MB-DNA. In order to improve the sensitivity, MB was designed to label with the recognition probe of Nb.*Bbv*CI directly.

3.6. Effect of the surface coverage of Au on the ECL intensity

Since the mechanism of the designed biosensor was based on the amount of recognition probes conjugated on Au particles surface, the ECL responses on the deposition voltage of Au were needed to be evaluated. Bare GCB was selected as a control. As can be seen in Fig. 5, ECL intensities exhibited no obvious change in the solution containing

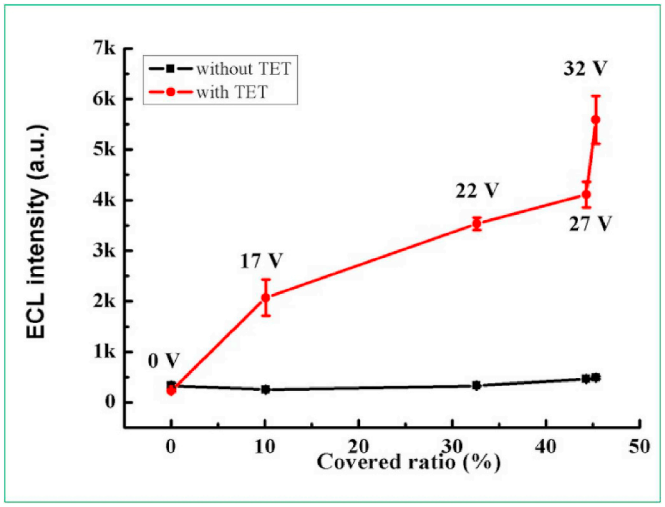

Fig. 5. ECL intensity as a function of cover ratio of Au on GCB. The plating voltage was ranged from 0 to 32 V. ECL intensities were recorded at aptamer/TET walker/MB-DNA/Au/GCB incubated with Nb.*Bbv*CI in the presence and absence of tetracycline.

bare GCBs in the absence and presence of TET. Additionally, the same background ECL intensities could be observed when aptamer/TET walker/MB-DNA/Au/GCB with various coverage area of Au was incubated with Nb.*Bbv*CI in the absence of TET, indicating that no MB-DNA was released from Au/GCB surface in the absence of TET. It

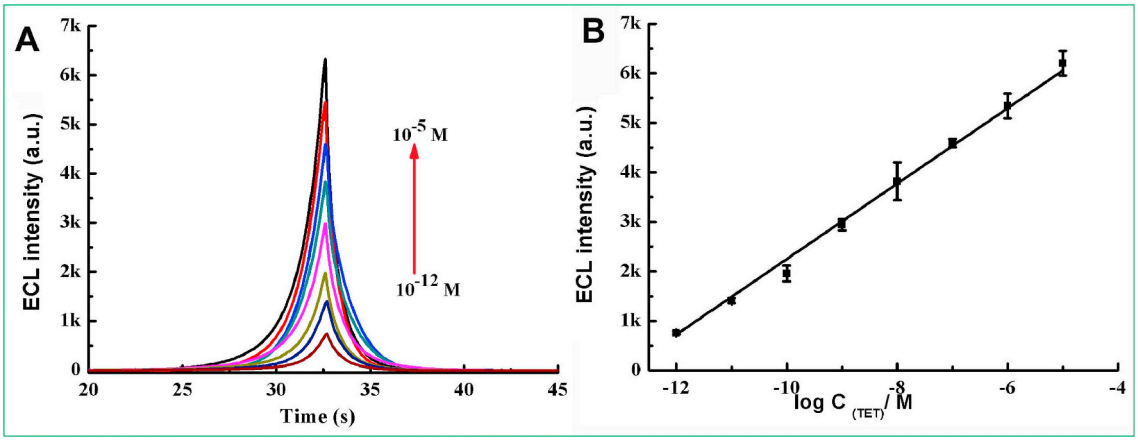

Fig. 6. (A) ECL-Time curves obtained in the presence of various concentration of TET from 10^{-12} to 10^{-5} M. (B) The linear relationship between ECL intensity and the logarithms of TET concentrations.

Table 1
Comparasion of various approaches for TET detection.

Method	Linear range	LOD	ref
Photoelectrochemical apatsensor	10–250 nM	5.3 nM	[44]
Fluorescent	50–1000 ng/mL	15.0 ng/mL	[50]
Electrochemistry	0.30–52.0 μM	0.10 μM	[51]
Colorimetric biosensor	100–1000 nM	45 nM	[52]
BPE biosensor	1×10^{-12} to 1×10^{-5} M	6×10^{-13} M	Present work

confirmed that the cleavage of MB-DNA was triggered by the presence of TET. Upon the incubation of TET, the change of ECL intensity ($\Delta I = I\text{-}I_0$, I and I_0 represented the ECL intensity recorded in the presence and absence of TET) was increased significantly with the increased deposition voltage of Au, attributing to the enlarged surface area of Au on GCB for the modification of DNA walker and MB-DNA according to Fig. 1. When the deposition voltage of Au was increased from 17 to 32 V, the coverage area was enlarged from 10.1 to 45.3% (see from Fig. 1), leading to an approximately 2.7-fold increase of ΔI. These results indicated that the coverage area of Au has a strong impact on the functionalization of biomolecules and the ECL intensity. In addition, each Au/GCB can be served as a biosensor to realize bioanalysis.

3.7. Calibration curve

Under the optimal conditions, ECL responses of different concentration of TET were performed when the deposition voltage of Au was 32 V. Fig. 6 displayed that the ECL intensity was increased as the concentration of TET increased. The linear range of the designed biosensor was from 1×10^{-12} to 1×10^{-5} M with the linear equation of $I = 9863 + 761.5 \log C$ ($R = 0.9968$). The detection limit was calculated to be 6.0×10^{-13} M, indicating the high sensitivity of the designed biosensor for the detection of TET. Compared with other assay, such as photoelectrochemistry [44], fluorescent [50], and electrochemistry [51], this biosensor shows a high sensitivity and low detection limit (Table 1).

The reproducibility of the biosensor for TET measurement was investigated with intra- and inter-assay precision. The intra-assay precision was evaluated by assaying one TET level for three reduplicate measurements, whereas the inter-assay precision was studied by measuring one TET level with three biosensors. The intra- and inter-assay variation coefficients for the detection of 1 nM TET were 1.2% and 4.5%, respectively, indicating acceptable reproducibility of the biosensor.

Table 2
Analytical recovery experiment of TET in milk sample by the designed biosensor.

Samples	Added (μM)	Found(μM)	RSD (%, n = 3)	Recovery (%)
1	0.100	0.103	3.9	103.1
2	0.500	0.469	5.8	93.8
3	1.00	0.960	1.5	95.9

3.8. Detection of TET in milk

Since TET may exist in food products, milk sample was chosen to evaluate the applicability of the designed biosensor using the standard addition method [53,54]. Different concentrations of standard TET were spiked into diluted milk samples and the results were displayed in Table 2. The recoveries were in the range from 93.8 to 103.1%, confirming the feasibility of the combination of single glassy carbon bead and closed BPE-ECL in real sample measurement.

4. Conclusions

We have successful fabricated area controllable sensing interface on a single glassy carbon bead and realize sensitive detection of tetracycline. The covered area of glassy carbon bead by Au particles is easily tailored by varying the deposition voltage in open bipolar electrochemical cell. Results have indicated that the ECL intensity is increased 2.7-fold when the area of Au was increased from 10.1 to 45.3%. Under the amplification effect of DNA walker and the reduction of methylene blue induced electrochemiluminescence (ECL) amplification strategy in closed BPE-ECL device, the designed biosensor displays excellent sensitivity and acceptable accuracy. Due to the outstanding merits of the proposed strategy, it shows great potential in sensitive and convenient detection of real sample.

Acknowledgment

This work was supported by the National Natural Science Foundation of China (No. 21675087).

References

[1] S. Hu, J. Gao, Wireless electroluminescence: polymer light-emitting electrochemical cells with inkjet-printed 1D and 2D bipolar electrode arrays, J. Phys. Chem. C 122 (16) (2018) 9054–9061.
[2] S. Hu, J. Gao, Dynamic bipolar electrode array for visualized screening of electrode materials in light-emitting electrochemical cells, Acs Appl. Mater. Inter. 11 (1) (2019) 1117–1124.

ARTICLE IN PRESS

[3] C. Liu, D. Wang, C. Zhang, A novel paperfluidic closed bipolar electrode-electrochemiluminescence sensing platform: potential for multiplex detection at crossing-channel closed bipolar electrodes, Sens. Actuators B Chem. 270 (2018) 341–352.

[4] H.-J. Lu, W. Zhao, J.-J. Xu, H.Y. Chen, Visual electrochemiluminescence ratiometry on bipolar electrode for bioanalysis, Biosens. Bioelectron. 102 (2018) 624–630.

[5] H. Motaghi, S. Ziyaee, M.A. Mehrgardi, A.A. Kajani, A.-K. Bordbar, Electrochemiluminescence detection of human breast cancer cells using aptamer modified bipolar electrode mounted into 3D printed microchannel, Biosens. Bioelectron. 118 (2018) 217–223.

[6] D. Wang, Y. Liang, Y. Su, Q. Shang, C. Zhang, Sensitivity enhancement of cloth-based closed bipolar electrochemiluminescence glucose sensor via electrode decoration with chitosan/multi-walled carbon nanotubes/graphene quantum dots-gold nanoparticles, Biosens. Bioelectron. 130 (2019) 55–64.

[7] Y. Wu, Y. Ren, Y. Tao, L. Hou, H. Jiang, High-throughput separation, trapping, and manipulation of single cells and particles by combined dielectrophoresis at a bipolar electrode array, Anal. Chem. 90 (19) (2018) 11461–11469.

[8] X. Zhang, N. Bao, X. Luo, S.-N. Ding, Patchy gold coated Fe3O4 nanospheres with enhanced catalytic activity applied for paper-based bipolar electrode-electrochemiluminescence aptasensors, Biosens. Bioelectron. 114 (2018) 44–51.

[9] L. Bouffier, S. Arbault, A. Kuhn, N. Sojic, Generation of electrochemiluminescence at bipolar electrodes: concepts and applications, Anal. Bioanal. Chem. 408 (25) (2016) 7003–7011.

[10] L. Bouffier, T. Doneux, B. Goudeau, A. Kuhn, Imaging redox activity at bipolar electrodes by indirect fluorescence modulation, Anal. Chem. 86 (8) (2014) 3708–3711.

[11] L. Bouffier, N. Sojic, A. Kuhn, Capillary-assisted bipolar electrochemistry: a focused mini review, Electrophoresis 38 (21) (2017) 2687–2694.

[12] A. de Poulpiquet, B. Diez-Buitrago, M. Milutinovic, B. Goudeau, L. Bouffier, S. Arbault, A. Kuhn, N. Sojic, Dual-color electrogenerated chemiluminescence from dispersions of conductive microbeads addressed by bipolar electrochemistry, Chemelectrochem 3 (3) (2016) 404–409.

[13] V. Essmann, D. Jambrec, A. Kuhn, W. Schuhmann, Linking glucose oxidation to luminol-based electrochemiluminescence using bipolar electrochemistry, Electrochem, Commun. Now. 50 (2015) 77–80.

[14] Z.A. Fattah, L. Bouffier, A. Kuhn, Indirect bipolar electrodeposition of polymers for the controlled design of zinc microswimmers, Appl. Mater. Today 9 (2017) 259–265.

[15] B. Gupta, B. Goudeau, P. Garrigue, A. Kuhn, Bipolar conducting polymer crawlers based on triple symmetry breaking, Adv. Funct. Mater. 28 (25) (2018).

[16] C. Kumsapaya, J. Limtrakul, A. Kuhn, D. Zigah, C. Warakulwit, Bipolar electrografting on the inner wall of carbon nanotubes, Chemelectrochem 3 (3) (2016) 410–414.

[17] G. Loget, J. Roche, E. Gianessi, L. Bouffier, A. Kuhn, Indirect bipolar electrodeposition, J. Am. Chem. Soc. 134 (49) (2012) 20033–20036.

[18] I. Malytska, T. Doneux, M. Bougouma, A. Kuhn, L. Bouffier, Wireless addressing of freestanding MoSe2 macro- and microparticles by bipolar electrochemistry, J. Phys. Chem. C 123 (9) (2019) 5647–5652.

[19] O. Phuakkong, M. Sentic, H. Li, C. Warakulwit, J. Limtrakul, N. Sojic, A. Kuhn, V. Ravaine, D. Zigah, Wireless synthesis and activation of electrochemiluminescent thermoresponsive janus objects using bipolar electrochemistry, Langmuir 32 (49) (2016) 12995–13002.

[20] B.-Y. Chang, K.-F. Chow, J.A. Crooks, F. Mavre, R.M. Crooks, Two-channel microelectrochemical bipolar electrode sensor array, Analyst 137 (12) (2012) 2827–2833.

[21] K.-F. Chow, B.-Y. Chang, B.A. Zaccheo, F. Mavre, R.M. Crooks, A sensing platform based on electrodissolution of a Ag bipolar electrode, J. Am. Chem. Soc. 132 (27) (2010) 9228–9229.

[22] K.-F. Chow, F. Mavre, J.A. Crooks, B.-Y. Chang, R.M. Crooks, A large-scale, wireless electrochemical bipolar electrode microarray, J. Am. Chem. Soc. 131 (24) (2009) 8364–+.

[23] S.E. Fosdick, R.M. Crooks, Bipolar electrodes for rapid screening of electrocatalysts, J. Am. Chem. Soc. 134 (2) (2012) 863–866.

[24] D. Hlushkou, R.K. Perdue, R. Dhopeshwarkar, R.M. Crooks, U. Tallarek, Electric field gradient focusing in microchannels with embedded bipolar electrode, Lab Chip 9 (13) (2009) 1903–1913.

[25] K.N. Knust, E. Sheridan, R.K. Anand, R.M. Crooks, Dual-channel bipolar electrode focusing: simultaneous separation and enrichment of both anions and cations, Lab Chip 12 (20) (2012) 4107–4114.

[26] E. Sheridan, D. Hlushkou, R.K. Anand, D.R. Laws, U. Tallarek, R.M. Crooks, Label-Free electrochemical monitoring of concentration enrichment during bipolar electrode focusing, Anal. Chem. 83 (17) (2011) 6746–6753.

[27] E. Sheridan, D. Hlushkou, K.N. Knust, U. Tallarek, R.M. Crooks, Enrichment of cations via bipolar electrode focusing, Anal. Chem. 84 (17) (2012) 7393–7399.

[28] X. Zhang, L. Zhang, Q. Zhai, W. Gu, J. Li, E. Wang, Self-powered bipolar electrochromic electrode arrays for direct displaying applications, Anal. Chem. 88 (5) (2016) 2543–2547.

[29] H. Xing, X. Zhang, Q. Zhai, J. Li, E. Wang, Bipolar electrode based reversible fluorescence switch using prussian blue/Au nanoclusters nanocomposite film, Anal. Chem. 89 (7) (2017) 3867–3872.

[30] W. Gao, K. Muzyka, X. Ma, B. Lou, G. Xu, A single-electrode electrochemical system for multiplex electrochemiluminescence analysis based on a resistance induced potential difference, Chem. Sci. 9 (16) (2018) 3911–3916.

[31] M.-S. Wu, Z. Liu, H.-W. Shi, H.-Y. Chen, J.-J. Xu, Visual electrochemiluminescence detection of cancer biomarkers on a closed bipolar electrode array chip, Anal. Chem. 87 (1) (2015) 530–537.

[32] M.-S. Wu, Z. Liu, J.-J. Xu, H.-Y. Chen, Highly specific electrochemiluminescence detection of cancer cells with a closed bipolar electrode, Chemelectrochem 3 (3) (2016) 429–435.

[33] H.-W. Shi, W. Zhao, Z. Liu, X.-C. Liu, M.-S. Wu, J.-J. Xu, H.-Y. Chen, Joint enhancement strategy applied in ECL biosensor based on closed bipolar electrodes for the detection of PSA, Talanta 154 (2016) 169–174.

[34] S. Ge, J. Zhao, S. Wang, F. Lan, M. Yan, J. Yu, Ultrasensitive electrochemiluminescence assay of tumor cells and evaluation of H_2O_2 on a paper-based closed-bipolar electrode by in-situ hybridization chain reaction amplification, Biosens. Bioelectron. 102 (2018) 411–417.

[35] X. Zhang, N. Bao, X.L. Luo, S.N. Ding, Patchy gold coated Fe3O4 nanospheres with enhanced catalytic activity applied for paper-based bipolar electrode-electrochemiluminescence aptasensors, Biosens. Bioelectron. 114 (2018) 44–51.

[36] J.-D. Zhang, N. Hao, L. Lu, S. Yun, X.-F. Zhu, K. Hong, L.-D. Feng, High-efficient preparation and screening of electrocatalysts using a closed bipolar electrode array system, J. Electroanal. Chem. 832 (2019) 1–6.

[37] S.M. Oja, B. Zhang, Electrogenerated chemiluminescence reporting on closed bipolar microelectrodes and the influence of electrode size, Chemelectrochem 3 (3) (2016) 457–464.

[38] Q. Zhai, X. Zhang, Y. Han, J. Zhai, J. Li, E. Wang, A nanoscale multichannel closed bipolar electrode array for electrochemiluminescence sensing platform, Anal. Chem. 88 (1) (2016) 945–951.

[39] S.G. Ge, J.G. Zhao, S.P. Wang, F.F. Lan, M. Yan, J.H. Yu, Ultrasensitive electrochemiluminescence assay of tumor cells and evaluation of H2O2 on a paper-based closed-bipolar electrode by in-situ hybridization chain reaction amplification, Biosens. Bioelectron. 102 (2018) 411–417.

[40] Q.-M. Feng, J.-B. Pan, H.-R. Zhang, J.-J. Xu, H.-Y. Chen, Disposable paper-based bipolar electrode for sensitive electrochemiluminescence detection of a cancer biomarker, Chem. Commun. 50 (75) (2014) 10949–10951.

[41] H.-W. Shi, M.-S. Wu, Y. Du, J.-J. Xu, H.-Y. Chen, Electrochemiluminescence aptasensor based on bipolar electrode for detection of adenosine in cancer cells, Biosens, Bioelectron 55 (2014) 459–463.

[42] B.Y. Chang, K.F. Chow, J.A. Crooks, F. Mavre, R.M. Crooks, Two-channel microelectrochemical bipolar electrode sensor array, Analyst 137 (12) (2012) 2827–2833.

[43] M. Wu, Y. Koizumi, H. Nishiyama, I. Tomita, S. Inagi, Buoyant force-induced continuous floating and sinking of Janus micromotors, RSC Adv. 8 (58) (2018) 33331–33337.

[44] Y. Liu, K. Yan, J.D. Zhang, Graphitic carbon nitride sensitized with CdS quantum dots for visible-light-driven photoelectrochemical aptasensing of tetracycline, ACS Appl. Mater. Interfaces 8 (42) (2016) 28255–28264.

[45] X.G. Liu, D.L. Huang, C. Lai, G.M. Zeng, L. Qin, C. Zhang, H. Yi, B.S. Li, R. Deng, S.Y. Liu, Y.J. Zhang, Recent advances in sensors for tetracycline antibiotics and their applications, Trac. Trends Anal. Chem. 109 (2018) 260–274.

[46] K. Wu, C. Ma, Z. Deng, N. Fang, Z. Tang, X. Zhu, K. Wang, Label-free and nicking enzyme-assisted fluorescence signal amplification for RNase H determination based on a G-quadruplexe/thioflavin T complex, Talanta 182 (2018) 142–147.

[47] F. Xuan, X.T. Luo, I.M. Hsing, Conformation-dependent exonuclease III activity mediated by metal ions reshuffling on thymine-rich DNA duplexes for an ultrasensitive electrochemical method for Hg^{2+} detection, Anal. Chem. 85 (9) (2013) 4586–4593.

[48] X. Zhang, Q. Zhai, L. Xu, J. Li, E. Wang, Paper-based electrochemiluminescence bipolar conductivity sensing mechanism: a critical supplement for the bipolar system, J. Electroanal. Chem. 781 (2016) 15–19.

[49] W. Gao, K. Muzyka, X. Ma, B. Lou, G. Xu, A single-electrode electrochemical system for multiplex electrochemiluminescence analysis based on a resistance induced potential difference, Chem. Sci. 9 (16) (2018) 3911–3916.

[50] L. Zhang, L. Chen, Fluorescence probe based on hybrid mesoporous silica/quantum dot/molecularly imprinted polymer for detection of tetracycline, ACS Appl. Mater. Interfaces 8 (25) (2016) 16248–16256.

[51] T. Gan, Z. Shi, J. Sun, Y. Liu, Simple and novel electrochemical sensor for the determination of tetracycline based on iron/zinc cations–exchanged montmorillonite catalyst, Talanta 121 (2014) 187–193.

[52] Y. Wang, Y. Sun, H. Dai, P. Ni, S. Jiang, W. Lu, Z. Li, Z. Li, A colorimetric biosensor using Fe_3O_4 nanoparticles for highly sensitive and selective detection of tetracyclines, Sens. Actuators B Chem. 236 (2016) 621–626.

[53] H. Tan, C. Ma, Y. Song, F. Xu, S. Chen, L. Wang, Determination of tetracycline in milk by using nucleotide/lanthanide coordination polymer-based ternary complex, Biosens. Bioelectron. 50 (2013) 447–452.

[54] Y. Luo, J. Xu, Y. Li, H. Gao, J. Guo, F. Shen, C. Sun, A novel colorimetric aptasensor using cysteamine-stabilized gold nanoparticles as probe for rapid and specific detection of tetracycline in raw milk, Food Control 54 (2015) 7–15.